Electronic structures of Ba$_{1-x}$Ca$_x$TiO$_3$ studied by x-ray absorption spectroscopy and theoretical calculation

Electronic structures of $Ba_{1-x}Ca_xTiO_3$ studied by x-ray absorption spectroscopy and theoretical calculation

K Asokan[1,5]**, J C Jan**[1]**, J W Chiou**[1]**, W F Pong**[1]**, M-H Tsai**[2]**, H L Shih**[1]**,
H Y Chen**[1]**, H C Hsueh**[1]**, C C Chuang**[1]**, Y K Chang**[3]**, Y Y Chen**[3] **and
I N Lin**[4]

[1] Department of Physics, Tamkang University, Tamsui 251, Taiwan, Republic of China
[2] Department of Physics, National Sun Yat-Sen University, Kaohsiung 804, Taiwan,
Republic of China
[3] Institute of Physics, Academia Sinica, Taipei 107, Taiwan, Republic of China
[4] Department of Materials Science and Engineering, Materials Science Center, National
Tsing-Hua University, Hsinchu 300, Taiwan, Republic of China

E-mail: asokan@nsc.ernet.in

Abstract

We report O and Ca K-edges x-ray absorption near edge structure (XANES)
spectra of $Ba_{1-x}Ca_xTiO_3$ ($x = 0.01$ and 0.08), $BaTiO_3$ and $CaTiO_3$ and
the electronic structure of $Ba_{0.875}Ca_{0.125}TiO_3$ obtained by first-principles
calculation. The characteristic features in the O K-edge XANES spectra of
these ferroelectric perovskites are influenced by the Ca concentration. They
differ substantially from those of the reference TiO_2. The O K-edge spectra
suggest that the combination of the alkaline-earth-metal oxides, CaO and/or
BaO, with TiO_2 enhance the effective charge of the O ions. Thus, a large
dipole moment may result from the displacement of the Ti ion from the centre
of the TiO_6 octahedron leading to collective displacement of Ti ions through
attractive dipole–dipole couplings and may give rise to ferroelectricity. In the
Ca K-edge XANES spectra there is a pre-edge feature similar to those found
in other 3d transition-metal perovskites, which may provide information about
hole doping.

1. Introduction

Barium titanate, $BaTiO_3$ (henceforth referred to as BTO), was the first perovskite-type
compound that showed ferroelectric transitions and to date is one of the most extensively
investigated ferroelectric materials [1]. It possesses a simple lattice structure allowing one
to employ a simple theoretical model to understand its ferroelectric property. In addition,
BTO proved to be an ideal material for many technological applications because of its

controllable electrical properties within a wide range of mixed crystal formation and doping. The characteristic feature of the titanate unit cell is a three-dimensional network of corner sharing TiO_6 octahedrons [2], which because of its high polarizability, essentially determines the dielectric property. BTO exhibits mainly three phase transitions of ferroelectric nature with decrease of temperature [1–3]. Despite extensive investigations, the origin of ferroelectricity and the nature of phase transitions in these perovskites are still not well understood [3]. The major complications arise from the fact that the amount of energy differences and displacements of ions involved in these phase transitions are very subtle. Often it was found that impurities, defects, stresses and grain size, domain formation and even light exposure could alter the transition temperature significantly [3], which suggested that the microscopic origin of this macroscopic phenomenon might be inferred from the electronic structures of these materials. Perovskite materials containing 3d transition metals (TMs) show very interesting dependence of their physical and chemical properties on the TM composition, temperature and pressure. The d–d interactions between 3d TM and alkaline-earth metals (AEMs) and the amount of covalent TM 3d–O 2p hybridization are also essential issues to be understood in these perovskites [4].

Previous studies of ferroelectric perovskites using x-ray absorption measurements focused on the equilibrium properties, Ti off-centre displacement as a function of the temperature and whether the phase transition is *order–disorder* or *displacive* type [5]. AEM oxides are important ingredients in perovskites. But, their roles have not been well understood. In these compounds Ca, Sr and Ba ions are known to induce charge carriers. They also give rise to a rich variety of physical properties in magnetism, ferroelectricity, superconductivity, metal–insulator transition and structural transformations [3, 4]. Ca-doped BTO has been used as a ceramic capacitor. It is a promising photorefractive material [6]. The main objective of this work is to understand the electronic structures of BTO with Ca substitutions by O and Ca K-edges absorption near edge structure (XANES) measurements. We report the electronic structures of $Ba_{1-x}Ca_xTiO_3$ ($x = 0.01$ and 0.08), $BaTiO_3$ and $CaTiO_3$ obtained by O and Ca K-edges XANES measurements and the electronic structure of $Ba_{0.875}Ca_{0.125}TiO_3$ obtained by first-principles calculation.

2. Experimental details

$Ba_{1-x}Ca_xTiO_3$ ($x = 0.01$ and 0.08), BTO and $CaTiO_3$ (henceforth referred to as CTO) samples were prepared from reagent grade $BaCO_3$, TiO_2 and $CaCO_3$ powders via standard ceramic routes. The characteristics of these samples were determined by x-ray diffraction, optical microscopy, electrical resistivity and dielectric constant measurements. The details of the preparation of these samples are given elsewhere [6]. Due to the low solubility of Ca in BTO and the formation of multiphase compounds, samples with the concentrations $x > 0.08$ are not included in our investigations. Room-temperature XANES spectra at O K-edges were recorded at high-energy spherical grating monochromator beamline and the Ca K-edge spectra at Si(111) double-crystal monochromator beamline at the Synchrotron Radiation Research Centre (SRRC) facility running at 1.5 GeV with a maximum stored current of 200 mA. Both these measurements were done in fluorescence mode using seven-element Ge detectors. The self-absorption corrections (SAC) were not applied for O K-edge measurements since it was known to be very small in this energy range and for oxides in general. Similarly, the concentrations of Ca were very low and only this mode can be utilized. We have not observed any saturation effect during these measurements and also the observed spectral features were consistent with other measurements reported in the literature (see section 4). Hence SAC were not applied in this investigation.

3. Theory

The density functional pseudopotential calculation [7] was carried out for BTO, CTO and $Ba_{0.875}Ca_{0.125}TiO_3$. The local density approximation based on the Perdew–Zunger parametrization was employed to describe the exchange-correlation interactions. The non-norm-conserving ultrasoft-pseudopotential using the Vanderbilt scheme [8, 9] was generated in the plane wave basis set. The CASTEP code (for details, see [7]) was used to perform full structural relaxation under the influence of *ab initio* forces and stress calculations. The equilibrium atomic positions of these compounds were determined by relaxation under the influence of Hellmann–Feynman forces. Furthermore, the external structural parameters (lattice constants, angles, etc) were optimized under the calculated stresses using the methods described in [10]. The core radii are chosen to be 1.58, 0.95, 0.84 and 0.53 Å for Ba, Ti, Ca and O, respectively. The structure of tetragonal symmetry (space group P4/mm) was employed. We used a 600 eV cut-off energy for the plane-wave basis set and a $4 \times 4 \times 4$ Monkhorst–Pack mesh of special k-points for better convergence [11]. The convergence of the calculated total energy was estimated to be better than 20 meV/atom. The equilibrium lattice geometry was determined by relaxing the influence of Hellmann–Feynman forces and stresses on the primitive unit cell [10]. The calculated equilibrium lattice constants, a (3.94 Å) and c (3.99 Å), for the tetragonal phase are less than 2% of the observed lattice constants of 3.99 and 4.03 Å, respectively [6]. The underestimate of lattice constants is mainly due to the 'over-binding' effect in local density approximations. To perform the electronic structure calculation for $Ba_{0.875}Ca_{0.125}TiO_3$, we have chosen a $2 \times 2 \times 2$ supercell, which contains eight primitive cells and 40 atoms. The supercell contains seven Ba atoms and one Ca atom. The calculated average Ba–O, Ca–O and Ti–O bond lengths are 2.66, 2.43 and 1.82 Å, respectively, which differ from the sum of their covalent radii, 2.71, 2.47 and 2.05 Å, respectively, by $\sim$2, 1.6 and 12%. The projected density of states (DOS) corresponding to each species of atoms was derived from the specific projections. Due to the limitations of our computational method, calculation was carried out only for the composition $x = 0.125$ not the $x = 0.08$ of the $Ba_{0.92}Ca_{0.08}TiO_3$ sample used in the XANES measurements. Since $x = 0.125$ does not differ much from $x = 0.08$, we hope the comparison between calculated and XANES results still useful. It may be noted that motivation behind this work has been focused on Ca doping in the BTO system and obtaining the essential features of both extreme members, namely BTO and CTO compounds. Our calculations for both BTO and CTO were consistent with Saha *et al* [12] and Ueda *et al* [13]. Moreover, a variety of calculations using different codes/methods exist in the literature for both BTO and CTO compounds and not for low-level Ca doping in BTO [3, 12, 13].

4. Results and discussion

The O K-edge XANES spectra of $Ba_{1-x}Ca_xTiO_3$ ($x = 0.01$ and 0.08), BTO, CTO and the reference TiO_2 samples are presented in figure 1. These spectra are normalized to have the same area in the energy range between 550 and 570 eV (not fully shown in the figure). After the background intensity in figure 1 was subtracted by a best-fit Gaussian line shape as shown by the dashed curve, five features marked by A_1, B_1, C_1, D_1 and E_1 in these spectra are identified. They are centred at $\sim$531, 533, 537, 540 and 544 eV, respectively. To show clearer the trend of the first two features A_1 and B_1, a magnified scale is shown in the inset of figure 1. Features A_1 and B_1 are well resolved for TiO_2. Similar two-peak feature at the threshold of the O K-edge XANES spectra were reported in other 3d-TM oxides [14, 15]. The overall intensities of features A_1 and B_1 remain more or less constant for $Ba_{1-x}Ca_xTiO_3$ ($x = 0.01$ and 0.08), BTO and CTO. For these compounds, the intensities of features A_1 and B_1, especially B_1, are
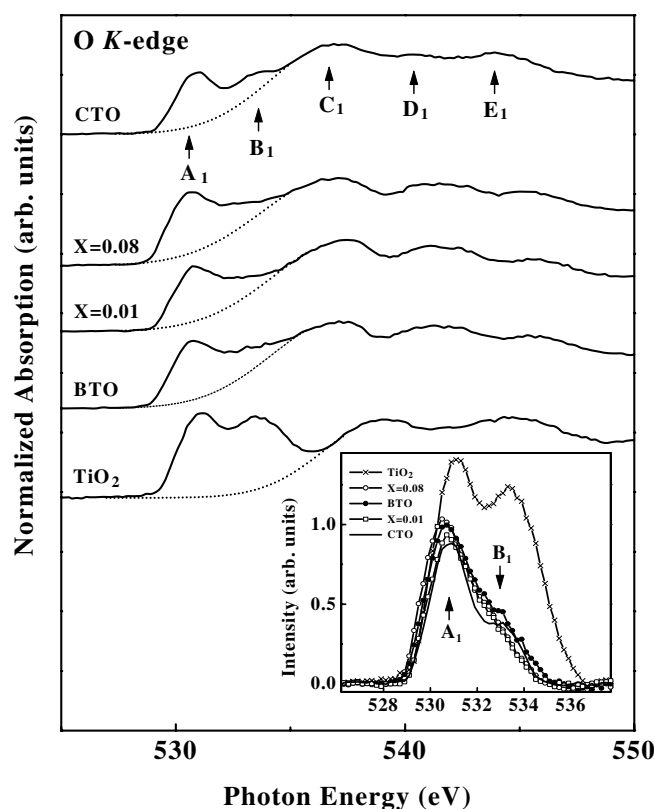
Figure 1. Normalized fluorescence yield at the O K-edge XANES spectra of $Ba_{1-x}Ca_xTiO_3$ ($x = 0.01$ and 0.08), BTO, CTO and TiO_2. The dashed curve is a best-fitted Gaussian shape background. The region containing features A_1 and B_1 after the background subtraction is shown in the inset on a magnified scale.

drastically reduced with respect to those for TiO_2. Besides, the energy positions of features A_1 and B_1 shift slightly towards the lower energy side relative to those for TiO_2. According to the dipole transition selection rules, the O K-edge XANES spectra reflect transitions from the O 1s core-state to the unoccupied oxygen 2p-derived states. Thus, the drastic reduction in the numbers of unoccupied O 2p states in $Ba_{1-x}Ca_xTiO_3$ implies an increase in the occupied O 2p states. This means an increase of the effective charge of the O ions in a cubic perovskites and demands TM ions to move from the centre of the octahedron. Consideration of tetragonal (or orthorhombic) symmetry allows one to conjecture that inequivalent effective charges on the O ions should dictate the Ti ions move from the centre of the octahedron and giving rise to a dipole. This in turn implies that a large dipole moment may form when the Ti ion is displaced from the centre of the TiO_6 octahedron, which enables collective displacement of the Ti ions through attractive dipole–dipole couplings and gives rise to ferroelectricity.

In figure 2, we compare the O K-edge XANES spectrum of $Ba_{0.92}Ca_{0.08}TiO_3$ and calculated oxygen p-projected DOS of $Ba_{0.875}Ca_{0.125}TiO_3$. The lower darkened area shows the theoretical oxygen p-projected DOS above the Fermi level. The upper solid curve is the O K-edge XANES spectra. The dashed curve in the middle is the theoretical oxygen p-projected DOS with the energy levels broadened by Lorentzian and Gaussian functions with widths of 0.3 eV to take into account core–hole lifetime and experimental broadening [16]. There is hybridization
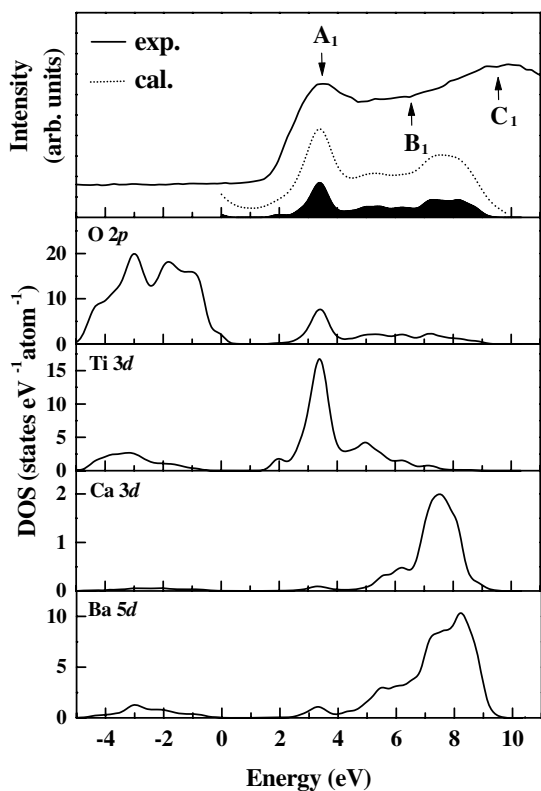
Figure 2. Comparison of the O K-edge XANES features for Ba$_{0.92}$Ca$_{0.08}$TiO$_3$ (upper solid curve) with the theoretical oxygen p-projected DOS for Ba$_{0.875}$Ca$_{0.125}$TiO$_3$ convoluted with core–hole lifetime and instrumental broadening. The spectra have been aligned at the position of the first peak and the intensity units have been normalized arbitrarily. The darkened area is the theoretical oxygen p-projected DOS above the Fermi level, which is defined as the zero energy.

between the O 2p and Ti 3d states within ∼6 eV above the Fermi level. The theoretical result for Ba$_{0.875}$Ca$_{0.125}$TiO$_3$ suggests that features A$_1$ and B$_1$ are primarily contributed by O 2p–Ti 3d t$_{2g}$ and e$_g$ hybridized states with a smaller contributions from O 2p–Ca 3d and O 2p–Ba 5d hybridized states. The significant hybridization between the Ti 3d and O 2p states suggests that Ti–O bonding in these systems are not purely ionic but contains a significant covalent part. The effect of the core–hole potential is more prominent for the e$_g$ band, which causes larger broadening of the e$_g$ band and feature B$_1$ through hybridization with the O 2p band [17–19]. As shown in the inset of figure 1 the intensity of feature B$_1$ is significantly smaller than that of feature A$_1$, which correlates with the calculated result that the e$_g$ band feature is much smaller than the t$_{2g}$ band feature. The integrated intensities of A$_1$ and B$_1$ features between 527 and 537.5 eV in the spectra of Ba$_{1-x}$Ca$_x$TiO$_3$ ($x = 0.01$ and 0.08) (2.6 and 3.0) and BTO (3.1) are slightly larger than that of CTO (2.5). This trend may be related to the change of the crystal structure from the tetragonal structure of Ba$_{1-x}$Ca$_x$TiO$_3$ ($x = 0.01$ and 0.08) and BTO to the orthorhombic structure of CTO [13]. The C$_1$ feature, which is absent in the spectrum of TiO$_2$ as shown in figure 1, arises from hybridization between the O 2p states and Ca 3d and Ba 5d states. The contributions from hybridization with the Ti and Ca 4sp and Ba 6sp states are much smaller than those with the Ti and Ca 3d and Ba 5d states and hence the projected DOS of these sp states are not shown in figure 2. Since our theoretical results for BTO and CTO were consistent with Saha *et al* [12] and Ueda *et al* [13] and these are not repeated here and compared with experimental results. However, the above spectral assignment and discussions are also valid for both BTO and CTO except that the spectral weights of Ba 5d states in BTO need to be replaced by Ca 3d states in CTO.
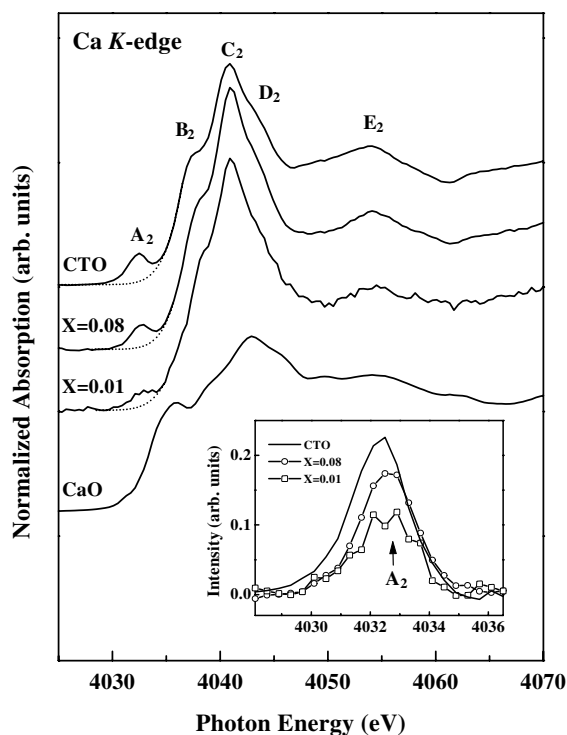
Figure 3. Normalized fluorescence yield at the Ca K-edge XANES spectra of $Ba_{1-x}Ca_xTiO_3$ (x = 0.01 and 0.08) and CTO. The dashed curve is a best-fitted Gaussian shape background. The region of feature A_2 after the background subtraction is shown in the inset on a magnified scale.

The normalized fluorescence yield Ca K-edge XANES spectra of $Ba_{1-x}Ca_xTiO_3$ (x = 0.01 and 0.08) and CTO are shown in figure 3. Within the energy region of interest of ∼30 eV above the edge, five features marked by A_2 to E_2 are identified after the background intensity in figure 3 was subtracted by a best-fitted Gaussian line shape as shown by the dashed curve. The inset in this figure highlights the increase in the spectral intensity of pre-edge feature A_2 with the Ca concentration. The spectral features A_2 to E_2 can be seen to change with the Ca concentration, which may be associated with the changes in the local environment and or charge transfer around Ca caused by the Ca substitution at the Ba site. Similar XANES features at the Ca K-edge were reported for CaF_2 and some garnets [20, 21]. The three most intense spectral features, B_2 to D_2, should arise mainly from Ca 1s → 4p transitions according to the dipole transition selection rule.

Figure 4 compares the Ca K-edge XANES spectrum of $Ba_{0.92}Ca_{0.08}TiO_3$ with the calculated Ca p-projected DOS of $Ba_{0.875}Ca_{0.125}TiO_3$. The darkened area shows the theoretical Ca p-projected DOS above the Fermi level. The upper solid curve is the Ca K absorption spectra at the region of XANES. The dashed curve in the middle is the theoretical Ca p-projected DOS obtained by broadening the energy levels with a Lorentzian function of width 0.81 eV and a Gaussian function of width 0.5 eV to simulate the core–hole lifetime and the experimental resolution, respectively [16]. Our calculational result shows that features C_2 and D_2 are dominantly contributed by the Ca 4p derived states. While feature B_2 is primarily contributed by O 2p–Ca 4p hybridized states. Our calculational result cannot explain feature E_2. One possible reason is that we did not use a large enough plane wave basis set, so that we did not have enough high-energy plane waves to adequately describe higher-energy Ca p states.

Pre-edge feature A_2 is still not well understood despite that various origins of this feature had been put forth previously [20, 21]. It is well known that the spectral features within ∼10 eV
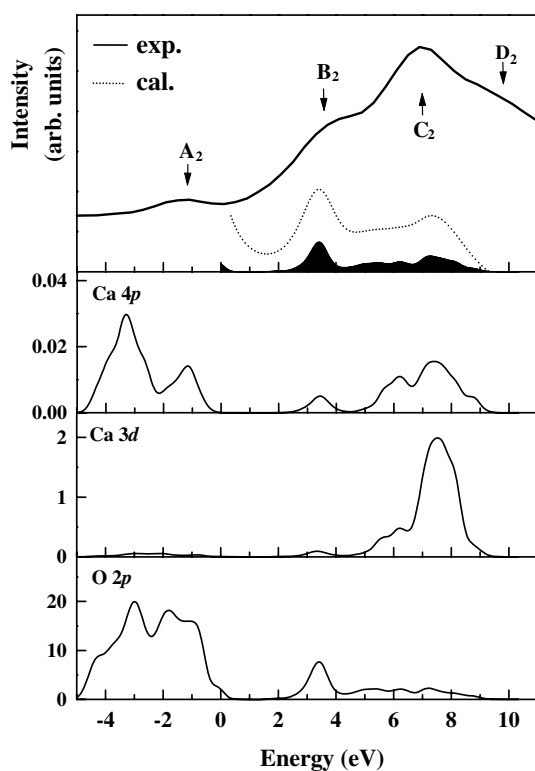
Figure 4. Comparison of the Ca K-edge XANES features for $Ba_{0.92}Ca_{0.08}TiO_3$ (upper solid-curve) with the theoretical Ca p-projected DOS for $Ba_{0.875}Ca_{0.125}TiO_3$ convoluted with core–hole lifetime and instrumental broadening.

of the edge threshold are due to electronic transitions to unoccupied states above the Fermi level. This region is sensitive to the details of the electronic potential due to the neighbouring ions that surround the Ca ion [22]. Pre-edge feature A_2 is commonly attributed to transitions from the Ca 1s states to bound Ca 3d or O 2p molecular orbitals. The transition to 3d orbitals is forbidden unless some d–p mixing is operating [23]. Distortion in the arrangement of the nearest neighbour (NN) oxygen atoms around the Ca ion is likely to occur in $Ba_{1-x}Ca_xTiO_3$. The Ca ions may cause considerable buckling and distortion in the crystal structure. Thus, the change in the intensity of the pre-edge feature in the Ca K-edge spectra as shown in the inset of figure 3 may arise from a NN oxygen configuration. Farges *et al* [24] proposed that the pre-edge feature at the K-edge could be attributed to multiple scattering effects and outlined a method for determining the coordination number of the Ca ion from this pre-edge information. Wu *et al* [25] demonstrated that the variation of the width and intensity of the pre-edge feature correlated with the occupation of the 3d band and the number of neighbouring atoms around the AEM site. A free Ca atom has an empty 3d shell. In BTO, the Ba ion is coordinated with 12 O ions, which suggests that the substitutional Ca ion in $Ba_{1-x}Ca_xTiO_3$ may have a similarly large coordination number. The large coordination number renders the coupling of the quadruple directional Ca 3d orbitals with neighbouring O 2p orbitals favourable. Then the Ca 3d–O 2p hybridized band may be broadened and extends to the valence band maximum (VBM) because the dominant part of the O 2p band of oxides is well known to be in the valence band. Our calculation implies that it is the case as shown in figure 4. The occupation of the Ca 3d derived states as shown in figure 4 shows that Ca 3d orbitals gain charge from valence-band O 2p orbitals, which gives rise to holes and contributes to feature A_2. Thus, feature A_2 in the Ca K-edge XANES spectra must be related to NN oxygen configuration. To

understand clearly, we have performed a calculation (without geometry optimization) fixing the position of the atoms. Our results (not shown here) indicates significant change in the O 2p states reflecting that the origin of the pre-edge peak is due to the arrangement of the NN oxygen atoms around the Ca ion. This study also indicates that the position of the A_2 peak corresponds to the top of the valence band dominated by O 2p states. Similar to the 3d TM K-edge XANES, the pre-edge feature gives information on the presence and the amount of the hole states [23, 26, 27]. Thus, the intensity of the pre-edge feature is related to the amount of hole doping in the system. This suggests that change in the intensity of the pre-edge feature in the Ca K-edge spectrum can be a common measure of the hole concentration in perovskites. It also provides a clue that AEMs play an important role in various phase transitions. AEMs not only are crucial for forming the perovskite structure but also tune the electronic structures of these materials. Our recent x-ray absorption measurements at the Ca $L_{2,3}$-edge also indicate that Ca 3d states are significantly low-lying, partially occupied and Ca may be regarded as low 3d TM [28, 29].

5. Conclusion

We have reported the experimental O and Ca K-edges XANES spectra of $Ba_{1-x}Ca_xTiO_3$ ($x = 0.01$ and 0.08), BTO and CTO and compared them with the theoretical results. The O K-edge XANES spectra display characteristic spectral features resulting predominantly from hybridization of the O 2p band with the Ti 3d t_{2g} and e_g bands. In comparison with the O K-edge spectrum of TiO_2, the intensities of the major features in the O K-edge spectra of $Ba_{1-x}Ca_xTiO_3$ were drastically reduced, which suggests an increase of the effective charge on the O ions. This effective charge of the O ions in cubic perovskites demands TM ions to move from the centre of octahedron. Consideration of tetragonal (or orthorhombic) symmetry allows one to conjecture that inequivalent effective charges on the O ions should dictate the Ti ions move from the centre of the octahedron and giving rise to a dipole. This in turn implies that a large dipole moment may form when the Ti ion is displaced from the centre of the TiO_6 octahedron, which enables collective displacement of the Ti ions through attractive dipole–dipole couplings and gives rise to ferroelectricity. The Ca K-edge XANES spectra have a pre-edge feature whose origin may be due to the arrangement of the NN oxygen atoms around the Ca ion. A similar feature is observed in 3d TM ions in the perovskites structure and it provides information about hole doping.

Acknowledgments

References

[1] Lines M E and Glass A M 1977 *Principles and Applications of Ferroelectrics and Related Materials* (Oxford: Oxford University Press)
[2] Kittel C 1996 *Introduction to Solid State Physics* (New York: Wiley)
[3] Cohen R E (ed) 2000 *Fundamental Physics of Ferroelectrics (AIP Proc.)*

Cohen R E 1992 *Nature* **359** 136

[4] Imada M, Fujimori A and Tokura Y 1998 *Rev. Mod. Phys.* **70** 1039

[5] Ravel B 1997 Ferroelectric phase transitions in oxide perovskites studied by XAFS *PhD Thesis* University of Washington

[6] Lin T F, Hu C T and Lin I N 1990 *J. Appl. Phys.* **67** 1042

[7] Payne M C, Teter M P, Allen D C, Arias T A and Joannopoulos J D 1992 *Rev. Mod. Phys.* **64** 1045

[8] Vanderbilt D 1990 *Phys. Rev.* B **41** 7892

[9] King-Smith R D and Vanderbilt D 1994 *Phys. Rev.* B **49** 5828

[10] Hsueh H C, Warren M C, Vass H, Ackland G J, Clark S J and Crain J 1996 *Phys. Rev.* B **53** 14 806

[11] Monkhorst H J and Pack J D 1976 *Phys. Rev.* B **13** 5188

[12] Saha S, Sinha T P and Mookerjee A 2000 *Phys. Rev.* B **62** 8828

[13] Ueda K, Yangi H, Hosono H and Kawazoc H 1999 *J. Phys.: Condens. Matter* **11** 3545

[14] de Groot F M F, Grioni M, Fuggle J C, Ghijsen J, Sawatzky G A and Petersen H 1989 *Phys. Rev.* B **40** 5715

[15] Pong W F *et al* 1996 *Phys. Rev.* B **54** 16 641

[16] See, Fuggle J C and Inglesfield J E (ed) 1992 *Unoccupied Electronic States* (Berlin: Springer) appendix B

[17] Brydson R, Sauer H, Engel W, Thomas J M, Zeitler E, Kosugi N and Kuroda H 1989 *J. Phys.: Condens. Matter* **1** 797

[18] Abbate M, Potze R, Sawatzky G A, Schlenker C, Lin H J, Tjeng L H, Chen C T, Teehan D and Turner T S 1995 *Phys. Rev.* B **51** 10 150

[19] Ruus R, Saar A, Aarik J, Aidla A, Uustare T and Kikas A 1998 *J. Electron Spectrosc. Relat. Phenom.* **92** 193

[20] Chaboy J and Quartieri S 1995 *Phys. Rev.* B **52** 6349

[21] Barkyoumb J H and Mansour A N 1992 *Phys. Rev.* B **46** 8768

[22] Stöhr J 1992 *NEXAFS Spectroscopy* (Berlin: Springer)

[23] Ravel B and Stern E A 1995 *Physica* B **208 & 209** 316

[24] Farges F, Brown G E and Rehr J J 1997 *Phys. Rev.* B **56** 1809

[25] Wu Z Y, Ouvard G, Moreau P and Natoli C R 1997 *Phys. Rev.* B **55** 9508

[26] Garcia J, Blasco J, Proietti M G and Benfatto M 1995 *Phys. Rev.* B **52** 15 823

[27] Vedrinskii R V, Kraizman V L, Novakovich A A, Demekhin Ph V and Urazhdin S V 1998 *J. Phys.: Condens. Matter* **10** 9561

[28] Nilsson P O and Forssell G 1977 *Phys. Rev.* B **16** 3352

[29] Asokan K, Jan J C, Chiou J W and Pong W F unpublished